Electric Supporting Information

Aspects of the selectivity, strengthen and sharpness in luminescence bands of lanthanide complexes from twenty-four praseodymium, europium and gadolinium complexes with differently distorted-hexadentate ligands

Miki Hasegawa*,[a,b], Shoya Sakurai,[a] Masafumi Andrew Yamaguchi,[a] Daichi Iwasawa,[a] Naho Yajima,[a] Shuhei Ogata,[a,b] Yudai Inazuka,[a] Ayumi Ishii[b,c,d] and Kengo Suzuki[e]

[a] *Department of Chemistry and Biological Science, College of Science and Engineering, Aoyama Gakuin University, 5-10-1 Fuchinobe, Chuo-ku, Sagamihara, Kanagawa 252-5258 Japan. E-mail: hasemiki@chem.aoyama.ac.jp; Fax: +81-42-759-6221*

[b] *Mirai Molecular Material Design Institute, Aoyama Gakuin University, 5-10-1 Fuchinobe, Chuo-ku, Sagamihara, Kanagawa 252-5258, Japan*

[c] *JST, PRESTO, 4-1-8 Honcho, Kawaguchi, Saitama 332-0012, Japan.*

[d] *Graduate School of Engineering, Toin University of Yokohama, Kurogane-cho, OAoba-ku, Yokohama, Kanagawa,225-8503, Japan*

[e] *Hamamatsu Photonics K. K., 812 Joko-cho, Higashi-ku, Hamamatsu, Shizuoka 341-3103, Japan*

Contents:

Table S1 Crystal parameters of PrL, PrL^{me}, PrL^{pr}, PrL^{dmpr}, EuL^{me}, EuL^{pr}, and EuL^{dmpr}.

Fig. S1. Packing structure of (a) PrL, (b) PrL^{me}, (c) PrL^{pr}, (d) PrL^{dmpr}, (e) EuL^{me}, (f) EuL^{pr}, and (g) EuL^{dmpr}.

Table S2 Selected inter atomic distances, angles and dihedral angles of EuL[1], EuL^{me} and EuL^{pr}, and EuL^{dmpr}.

Fig. S2. Excitation spectra of (a) EuL^{me}, (b) EuL^{pr}, (c) EuL^{dmpr}, (d) EuL^{me}H. (e) EuL^{pr}H and (f) EuL^{dmpr} in the solid (dotted-line) and in acetonitrile (solid-line).

Fig. S3. Luminescence decay profiles monitored at the $^5D_0$-$^7F_2$ transition of Eu ion for (a) EuL^{me}, (b) EuL^{pr} and (c) EuL^{dmpr}, (d) EuL^{me}H, (d) EuL^{pr}H and (e) EuL^{dmpr}H in the solid and in acetonitrile.

Fig. S4. Illustrated comparison between radiative- (Arad; sky-blue), nonradiative- (Anr; orange) rate constants and energy transfer efficiency (ηsense) of a series of Eu complexes in heliate ligands.

Calculation of energy transfer efficiency by the Judd-Ofelt theory to evaluate luminescence of Eu complexes. [2-4]

Fig. S5. Luminescence spectra of (a, e) EuLH^{52}, (b, f) $\mathrm{EuL^{me}H}$, (c, g) $\mathrm{EuL^{pr}H}$, and (d, h) $\mathrm{EuL^{dmpr}H}$ in the solid (left column) and in acetonitrile (right column). Inset shows the $^5D_0 \rightarrow {}^7F_1$ band. λ_{ex} =300 nm.

Fig. S6. Excitation spectra of (a) PrL, (b) $\mathrm{PrL^{me}}$, (c) $\mathrm{PrL^{pr}}$, (d) $\mathrm{PrL^{dmpr}}$, (e) PrLH, (f) $\mathrm{PrL^{me}H}$. (g) $\mathrm{PrL^{pr}H}$, (h) $\mathrm{PrL^{dmpr}}$ in the solid (dotted-line) and in acetonitrile (solid-line).

Table S3 Wavelength positions of fluorescence and phosphorescence bands of a series of Gd complexes in the solid state, acetonitrile (for at rt) and ethanol (for at 77 K). "sh" means the shoulder position of the phosphorescence band.

Fig. S7. Band assignment of ff transitions in luminescence spectrum of Pr complexes (PrL), and Energy diagram of trivalent Pr ion. [5]

Fig. S8. NIR-luminescence spectra of Pr complexes recorded on Hamamatsu Photonics C9920. λ_{ex} = 300-400 and 475 nm.

Table S4 Excitation wavelength dependences on QY in NIR luminescence of Pr complexes.

Fig. S9. ^{1}H-NMR spectra of (a) $\mathrm{L^{me}}$, (b) $\mathrm{L^{pr}}$, and (c) $\mathrm{L^{dmpr}}$, (d) $\mathrm{L^{me}H}$, (e) $\mathrm{L^{pr}H}$, and (f) $\mathrm{L^{dmpr}}$ H in $\mathrm{CDCl_3}$.

References

Table S1 Crystal parameters of PrL, PrL^{me}, PrL^{pr}, PrL^{dmpr}, EuL^{me}, EuL^{pr}, and EuL^{dmpr}.

Ln	PrL	PrL^{me}	PrL^{pr}	PrL^{dmpr}	EuL^{me}	EuL^{pr}	EuL^{dmpr}
Formula	$C_{26}H_{23}F_6N_9O_6PPr$	$C_{27}H_{24}F_6N_9O_6PPr$	$C_{27}H_{24}F_6N_9O_6PPr$	$C_{29}H_{29}F_6N_9O_6PPr$	$C_{27}H_{25}EuF_6N_9O_6P$	$C_{27}H_{24}EuF_6N_9O_6P$	$C_{27}H_{26}EuF_6N_8O_6P$
Formula weight	843.41	857.44	857.44	885.49	868.49	868.49	855.49
Crystal size (mm)	0.47x0.38x0.32	0.400x0.350x0.300	0.226x0.210x0.178	0.376x0.238x0.227	0.303x0.239x0.197	0.372x0.372x0.272	0.400x0.365x0.234
Crystal system	Triclinic	monoclinic	monoclinic	Triclinic	Monoclinic	Monoclinic	Orthorhombic
Space group	P-1	C2/c	P 21/n	*P*-1	C2/c	P 21/n	Pbca
a (Å)	8.9374(5)	24.6944(13)	13.1861(9)	11.2569(6)	24.708(3)	13.2647(9)	16.7522(18)
b (Å)	12.2439(6)	12.1525(7)	11.8048(8)	12.6567(7)	12.1202(12)	11.7465(8)	14.5415(15)
c (Å)	16.3426(9)	24.3587(18)	20.6297(14)	13.6840(8)	24.378(3)	20.5653(14)	25.718(3)
α (˚)	110.1560(10)	90	90	63.881(1)	90	90	90
β (˚)	105.64	119.0850(10)	96.8230	88.073(1)	119.7230(10)	96.9060(10)	90
γ (˚)	92.5860(10)	90	90	85.069(1)	90	90	90
V (Å^3)	1597.73(15)	6388.2(7)	3188.5(4)	1744.04(17)	6339.89(7)	3181.1(4)	6264.96(11)
Z value	2	8	4	2	8	4	8
D_{calcd} (Mg m^{-3})	1.753	1.783	1.786	1.686	1.820	1.813	1.814
μ (Mo Ka) (mm^{-1})	1.665	1.668	1.671	1.530	2.122	2.115	2.145
F(000)	836	3408	1704	884	3440	1720	3392
λ (Mo Ka) (Å)	0.71073	0.71073	0.71073	0.71073	0.71073	0.71073	0.71073
Temperature (K)	90	90	90	90	90	90	90
R1^a (I > 2.00s(I))	0.0295	0.0340	0.0640	0.0276	0.0439	0.0198	0.0228
wR2^b (I > 2.00s(I))	0.0819	0.0753	0.1540	0.0696	0.0950	0.0497	0.0565
Goodness of fit	1.075	1.213	1.098	1.035	1.394	1.052	1.026
Largest peak and hole (e Å^{-3})	3.307, -1.227	1.995, -1.118	3.665, -2.568	2.015, -1.275	1.191, -1.886	1.952, -1.889	0.661, -0.560

Fig. S1. Packing structure projected from the *b*-axis of (a) PrL, (b) $\mathrm{PrL^{me}}$, (c) $\mathrm{PrL^{pr}}$, (d) $\mathrm{PrL^{dmpr}}$, (e) $\mathrm{EuL^{me}}$, (f) $\mathrm{EuL^{pr}}$, and (g) $\mathrm{EuL^{dmpr}}$.

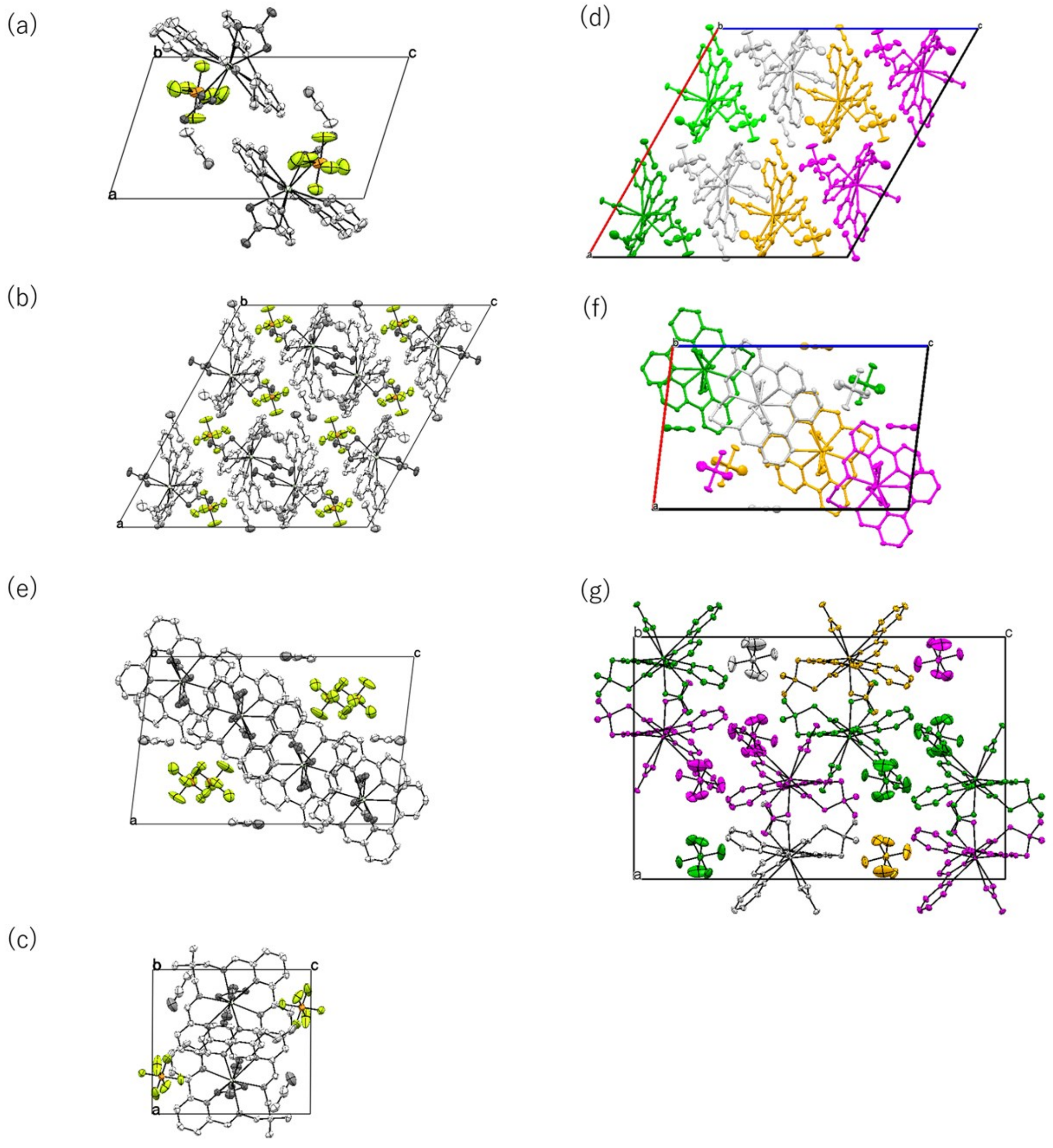

Table S2 Selected interatomic distances, angles and dihedral angles of PrL, PrL^{me}, PrL^{pr}, PrL^{dmpr}, EuL^{me}, EuL^{pr} and EuL^{dmpr}.

	PrL	PrL^{me}	PrL^{pr}	PrL^{dmpr}	EuL^{me}	EuL^{pr}	EuL^{dmpr}
Mean N$_{bpy}$-Pr/Eu distances/ Å	2.653	2.655	2.568	2.651	2.592	2.591	2.575
Mean N$_{bridge}$-Pr/Eu distances / Å	2.585	2.599	2.593	2.621	2.550	2.547	2.560
Mean O-Pr/Eu distances / Å	2.556	2.561	2.579	2.564	2.508	2.528	2.525
Distance N3-N4 / Å	2.732	2.719	2.894	2.895	2.680	2.842	2.703
Dihedral angle* / ⁰	31.8	50.5	55.6	43.3	50.9	53.9	71.1

* Dihedral Angle between Ln1N1N2N3 and Ln1N6N5N4 (Ln=Pr or Eu)

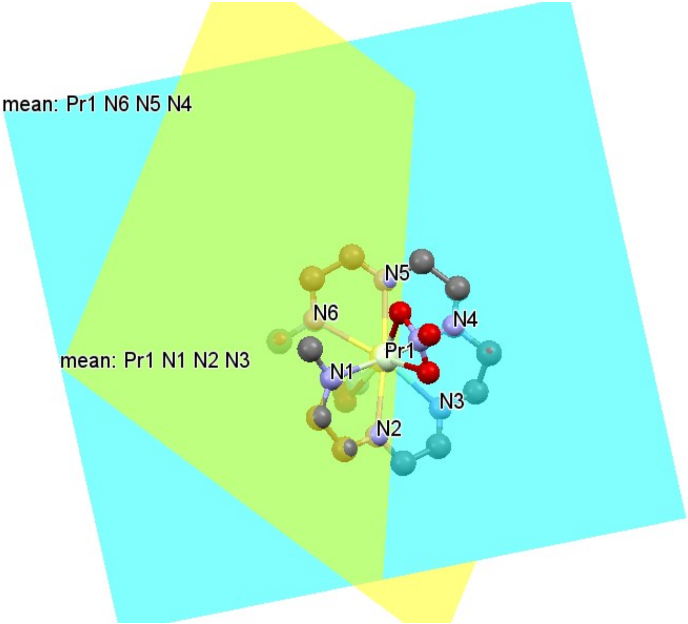

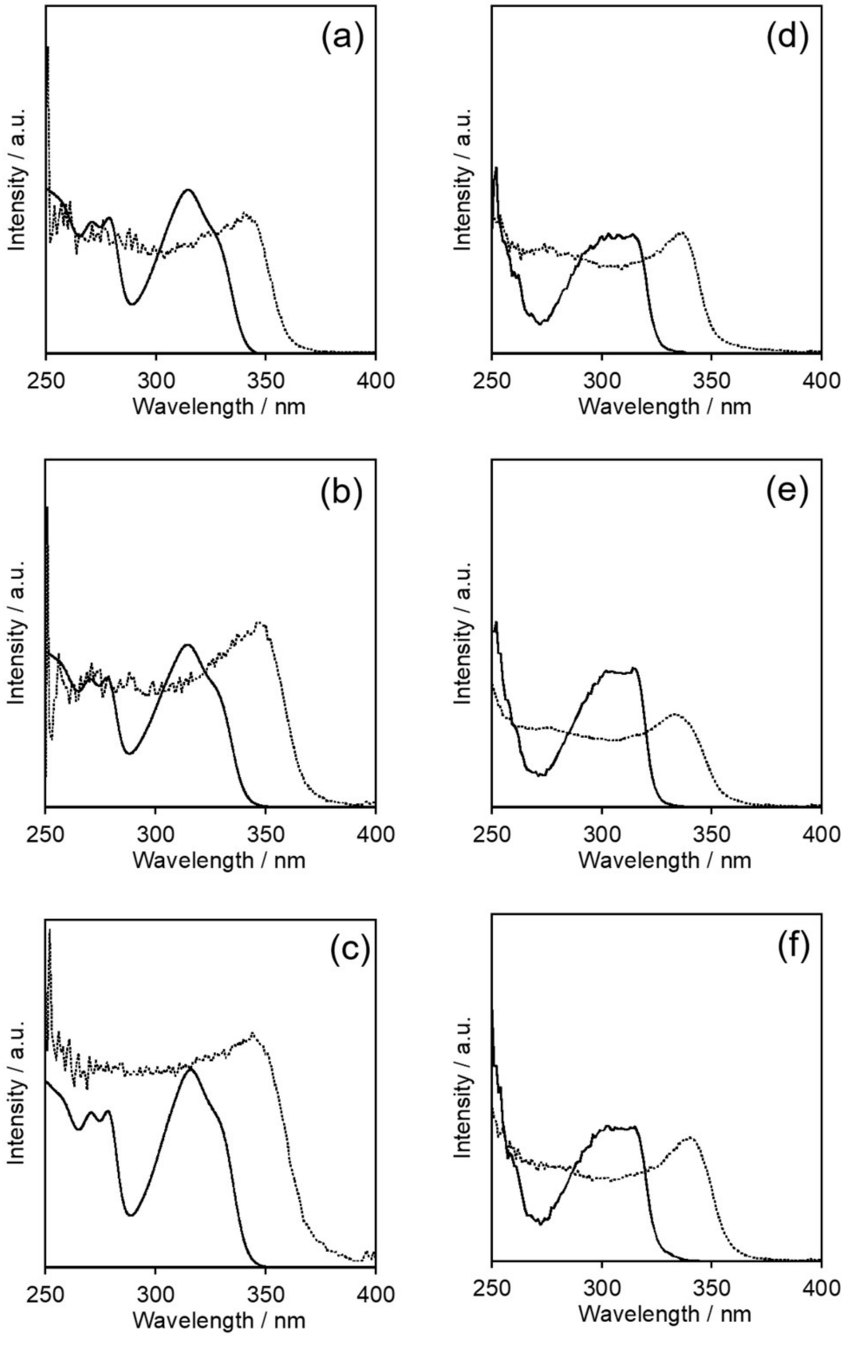

Fig. S2. Excitation spectra of (a) EuL^{me}, (b) EuL^{pr}, (c) EuL^{dmpr}, (d) $EuL^{me}H$. (e) $EuL^{pr}H$ and (f) EuL^{dmpr} in the solid (dotted-line) and in acetonitrile (solid-line).

Table S3 Wavelength positions of fluorescence and phosphorescence bands of a series of Gd complexes in the solid state, acetonitrile (for at rt) and ethanol (for at 77 K). “sh” means the shoulder position of the phosphorescence band.

	Fluorescence (at rt)		Phosphorescence (at 77 K)			
	in solution	Solid state	in solution		Solid state	
GdL	353 nm	364	500	480 (sh)	506	470 (sh)
$\mathrm{GdL^{me}}$	355	363	498	460 (sh)	523	470 (sh)
$\mathrm{GdL^{pr}}$	356	368	497	470 (sh)	505	470 (sh)
$\mathrm{GdL^{dmpr}}$	357	364	508	475 (sh)	508	475 (sh)
GdLH	335	355	494	440 (sh)	500	440 (sh)
$\mathrm{GdL^{me}H}$	336	359	502	440 (sh)	510	460 (sh)
$\mathrm{GdL^{pr}H}$	337	360	497	430 (sh)	497	430 (sh)
$\mathrm{GdL^{dmpr}H}$	338	352	498	445 (sh)	510	445 (sh)

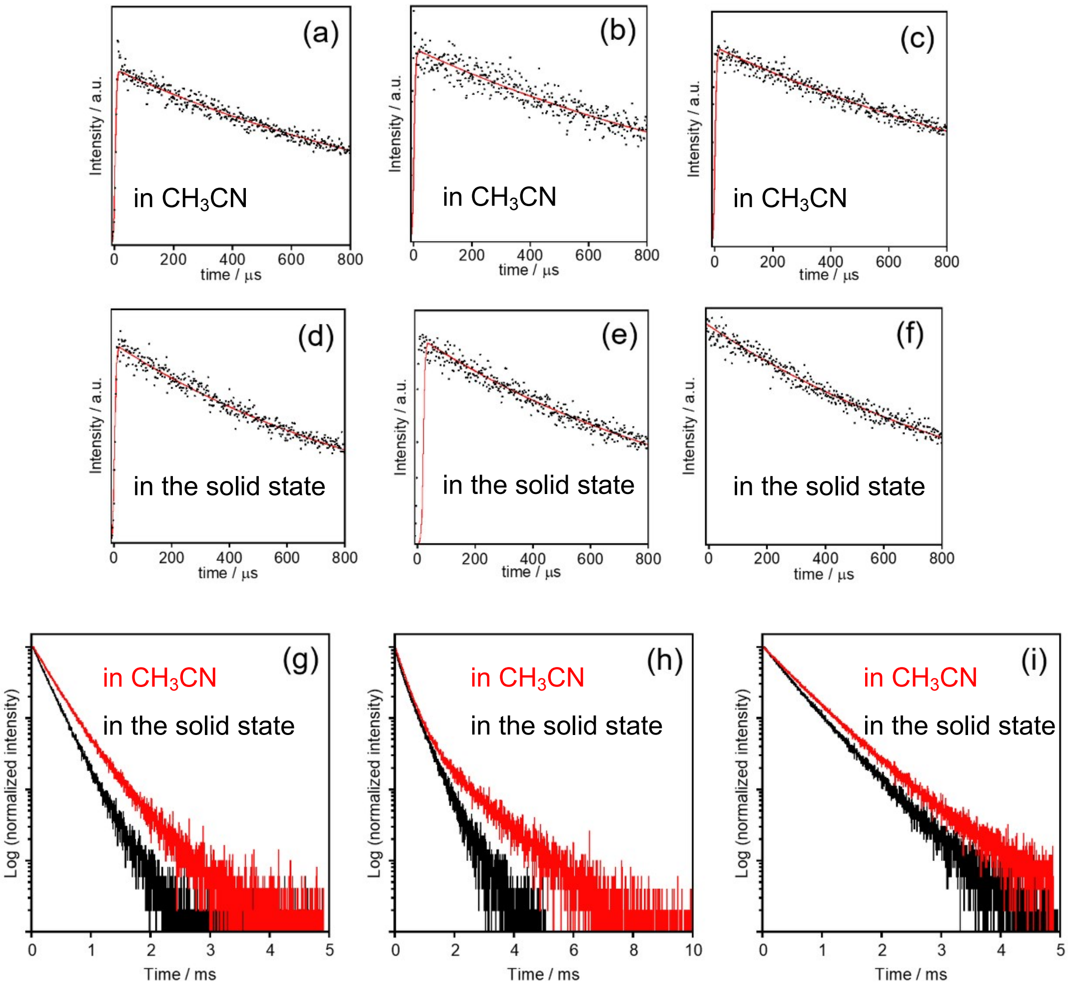

Fig. S3. Luminescence decay profiles monitored at the $^5D_0$-$^7F_2$ transition of Eu ion for EuL^{me}((a); in acetonitrile, (d); in the solid state), EuL^{pr} ((b); in acetonitrile, (e); in the solid state) and EuL^{dmpr}((c); in acetonitrile, (f); in the solid state). (g), (h) and (i) are luminescence decay profiles of EuL^{me}H, EuL^{pr}H and EuL^{dmpr}H, respectively, in the solid state and acetonitrile.

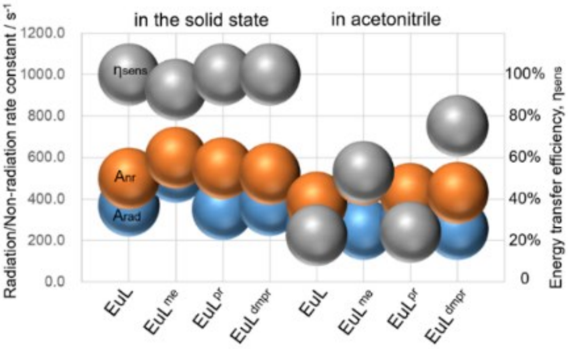

Fig. S4. Illustrated comparison between radiative- (A_{rad}; sky-blue), nonradiative- (A_{nr}; orange) rate constants and energy transfer efficiency (η_{sense}) of a series of Eu complexes in heliate ligands.

Calculation of energy transfer efficiency by the Judd-Ofelt theory to evaluate luminescence of Eu complexes.[2-4]

The luminescence efficiency of Eu ion sensitized by the ligand (φ_{ff}) is determined by the triplet yield of the ligand (φ_{ISC}), the efficiency of the energy transfer (η_{EnT}) and the efficiency of the metal-centered luminescence (η_{Ln}), as follows.

$$\phi_{\mathrm{ff}} = \phi_{\mathrm{ISC}} \times \eta_{\mathrm{EnT}} \times \phi_{\mathrm{Ln}} \tag{1}$$

Based on the nπ* character of the ligand and the high spin-orbit coupling constants of the lanthanide ion, the φ_{ISC} value of approximately 1 can be assumed. The value of φ_{Ln} can then be calculated from the experimentally observed emission lifetime (τ_{ff}) and the radiative rate constant (k_{R}) of the lanthanide ion, as shown below.

$$\phi_{\mathrm{Ln}} = k_{\mathrm{R}} \times \tau_{\mathrm{ff}} \tag{2}$$

The k_{R} value of the emissive excited state, $^5D_0$, is the sum of the spontaneous emission probabilities, $A_J(0, J)$, to the lower ^7F_J levels in Eu^{3+}, and can in turn be calculated using the following equation.

$$k_{\mathrm{R}} = \sum A_J(0,J) = A_{\mathrm{MD}} \times \sum A_{\mathrm{ED}} \tag{3}$$

Here, the spontaneous emission probability of the magnetic dipole $^5D_0 \rightarrow {}^7F_1$ transition, A_{MD}, is virtually independent of the ligand field or the environment of the ions, and can be determined directly from the theoretically calculated dipole strength as follows.

$$A_{\mathrm{MD}} = \frac{64\pi^4 \sigma_{MD}^3 n^3}{3h(2J+1)} \times S_{\mathrm{MD}} \tag{4}$$

In the above, σ_{MD} is the energy gap between the excited ($^5D_0$) and final ($^7F_1$) states (with a value of 16949.2 cm^{-1}), n is the refractive index (1.5 for the solid state and 1.34 for acetonitrile [3,4]) and S_{MD} is the magnetic dipole strength. The latter parameter has been calculated theoretically for the $^5D_0 \rightarrow {}^7F_1$ transition of Eu^{3+} and found to have a value of 9.60×10^{-42} esu^2cm^2, resulting in a value of 37.93 s^{-1} for A_{MD}.

A_{ED} in equation (3) is the emission probability associated with the electric dipole transition, as determined using the Judd-Ofelt parameter (Ω_λ) in the equation below.

$$A_{\mathrm{ED}} = \frac{64\pi^4 e^2 \sigma_J^3}{3h(2J+1)} \frac{n(n^2+2)^2}{9} \times \sum\nolimits_{\lambda=2,4} \Omega_\lambda \left| \left\langle \psi J \middle\| U^{(\lambda)} \middle\| \psi' J' \right\rangle \right|^2 \tag{5}$$

Ω_λ is, in turn, calculated from the following equation.

$$\Omega_\lambda = \frac{S_{\mathrm{MD}}}{e^2} \frac{\sigma_{MD}^3}{\sigma_J^3} \frac{9n^2}{(n^2+2)^2 \left| \left\langle \psi J \middle\| U^{(\lambda)} \middle\| \psi' J' \right\rangle \right|^2} \frac{\int I_J(\nu) d\nu}{\int I_{MD}(\nu) d\nu} \tag{6}$$

Here, $\int I_J \, dv / \int I_{\mathrm{MD}} \, dv$ is the ratio of the integrated intensity of the corrected Eu^{3+} luminescence spectrum ($^5D_0 \rightarrow {}^7F_J : J = 0, 1, 2, 3$ and 4) to the intensity of the $^5D_0 \rightarrow {}^7F_1$ band, and $|\langle \Psi J \| U^{(\lambda)} \| \Psi' J' \rangle|$ is the tensor operator [5]. Based on the Judd-Ofelt analysis, it is able to estimate A_{ED} value for the $^5D_0 \rightarrow {}^7F_2$ transition, using the k_{R} value obtained from equation (3). The non-radiative rate constant (k_{NR}) can be estimated using the relationship below.

$$k_{\mathrm{NR}} = \frac{1}{\tau_{\mathrm{obs}}} - k_{\mathrm{R}} \tag{7}$$

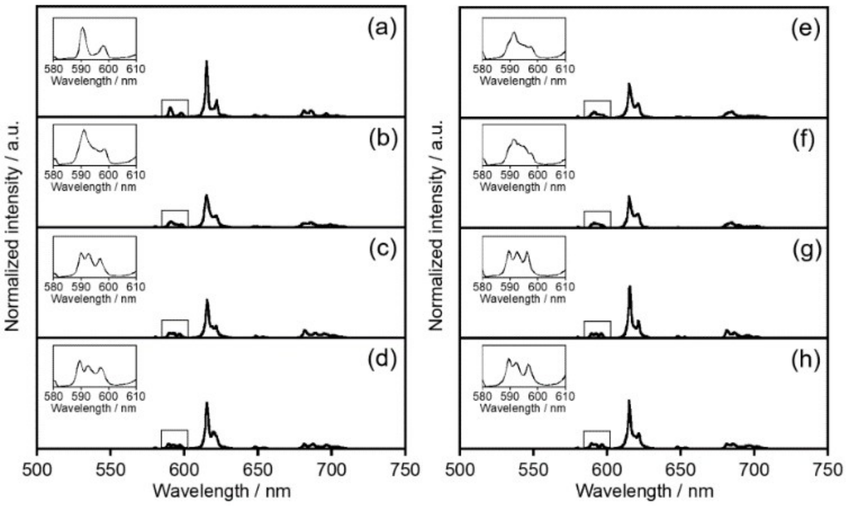

Fig. S5. Luminescence spectra of (a, e) EuLH[56,57], (b, f) EuL^{me}H, (c, g) EuL^{pr}H, and (d, h) EuL^{dmpr}H in the solid (left column) and in acetonitrile (right column). Inset shows the $^5D_0 \rightarrow {}^7F_1$ band. λ_{ex} =300 nm.

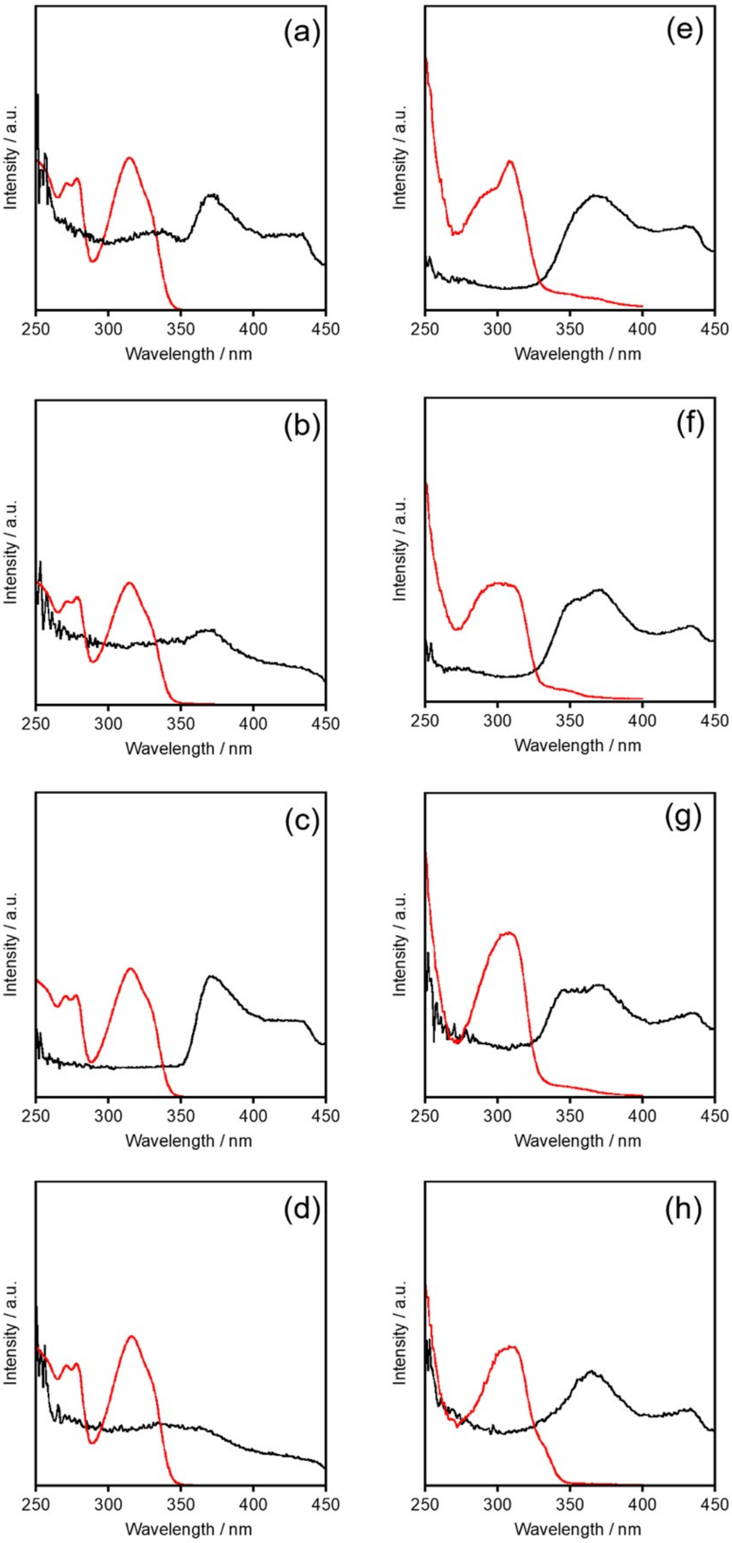

Fig. S6. Excitation spectra of (a) PrL, (b) PrL^{me}, (c) PrL^{pr}, (d) PrL^{dmpr}, (e) PrLH, (f) PrL^{me}H. (g) PrL^{pr}H, (h) PrL^{dmpr}H in acetonitrile (red) and in the solid state (black).

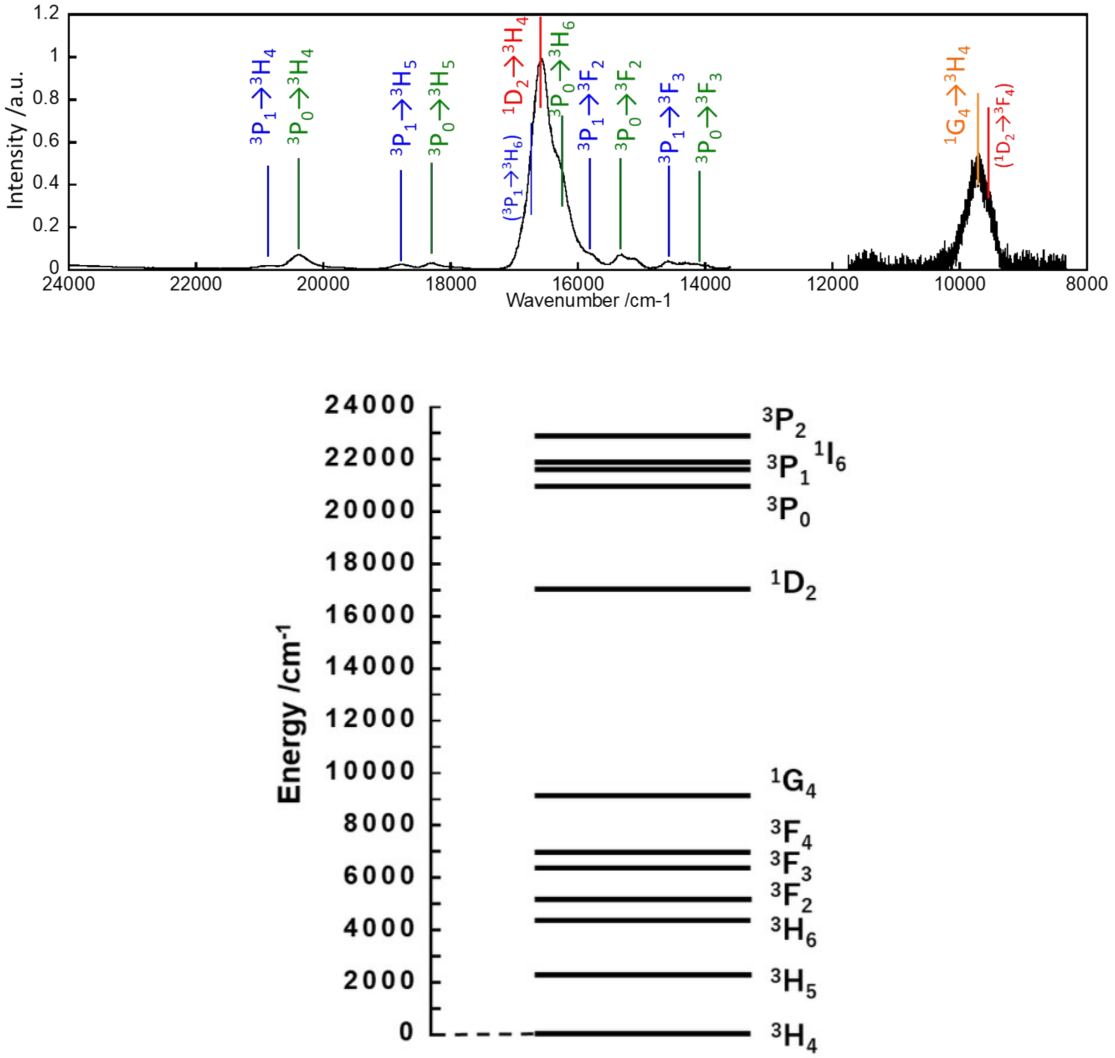

Fig. S7. Band assignment of ff transitions in luminescence spectrum of Pr complexes (PrL), and Energy diagram of trivalent Pr ion. [5]

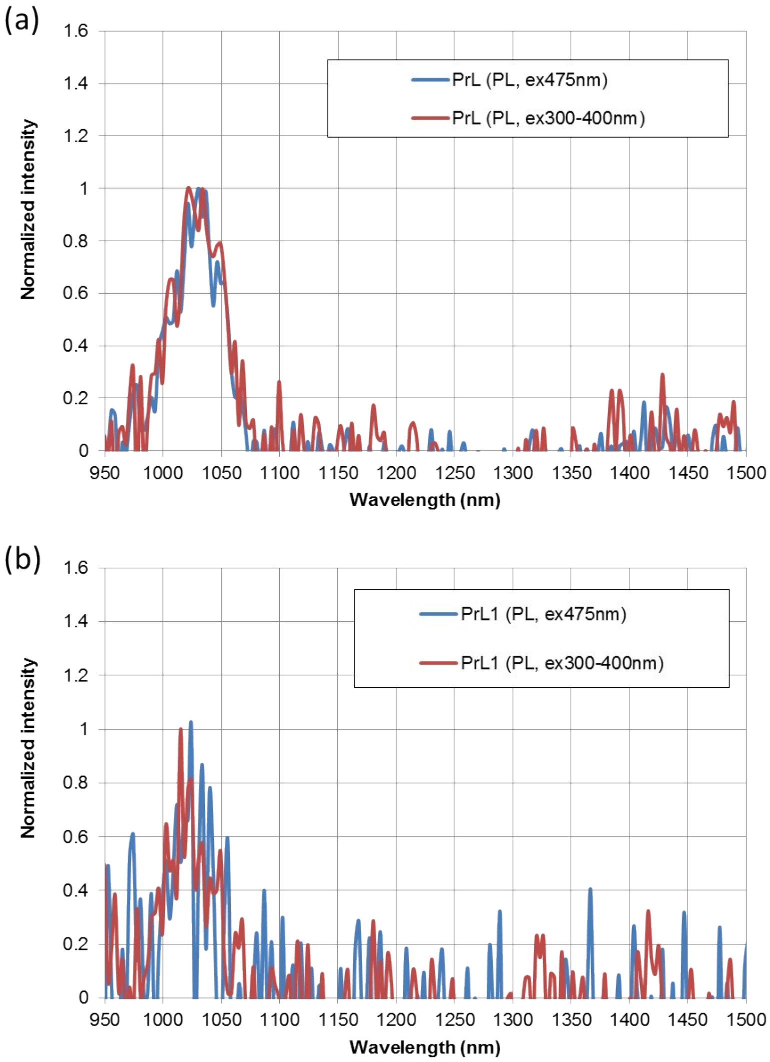

Fig. S8. NIR-luminescence spectra of Pr complexes, (a) PrL and (b) PrL^{pr} in the solid state recorded on Hamamatsu Photonics C9920. λ_{ex} = 300-400 and 475 nm.

Table S4 Excitation wavelength dependences on QY in NIR luminescence of Pr complexes.

	λ_{mon} = 480-850 nm	λ_{mon} = 980 - 1080 nm	
	λ_{ex} = 330 nm	λ_{ex} = 330 nm	λ_{ex} = 475 nm
PrL	1.0%	0.006%	0.008%
PrL^{me}	-	0.001%	0.002%
PrL^{pr}	1.3%	0.004%	0.004%
PrL^{dmpr}	-	0.009%	0.010%

Fig. S9. ^{1}H-NMR of (a) L^{me}, (b) L^{pr}, and (c) L^{dmpr}, (d) $L^{me}H$, (e) $L^{pr}H$, and (f) L^{dmpr} H in $CDCl_3$.

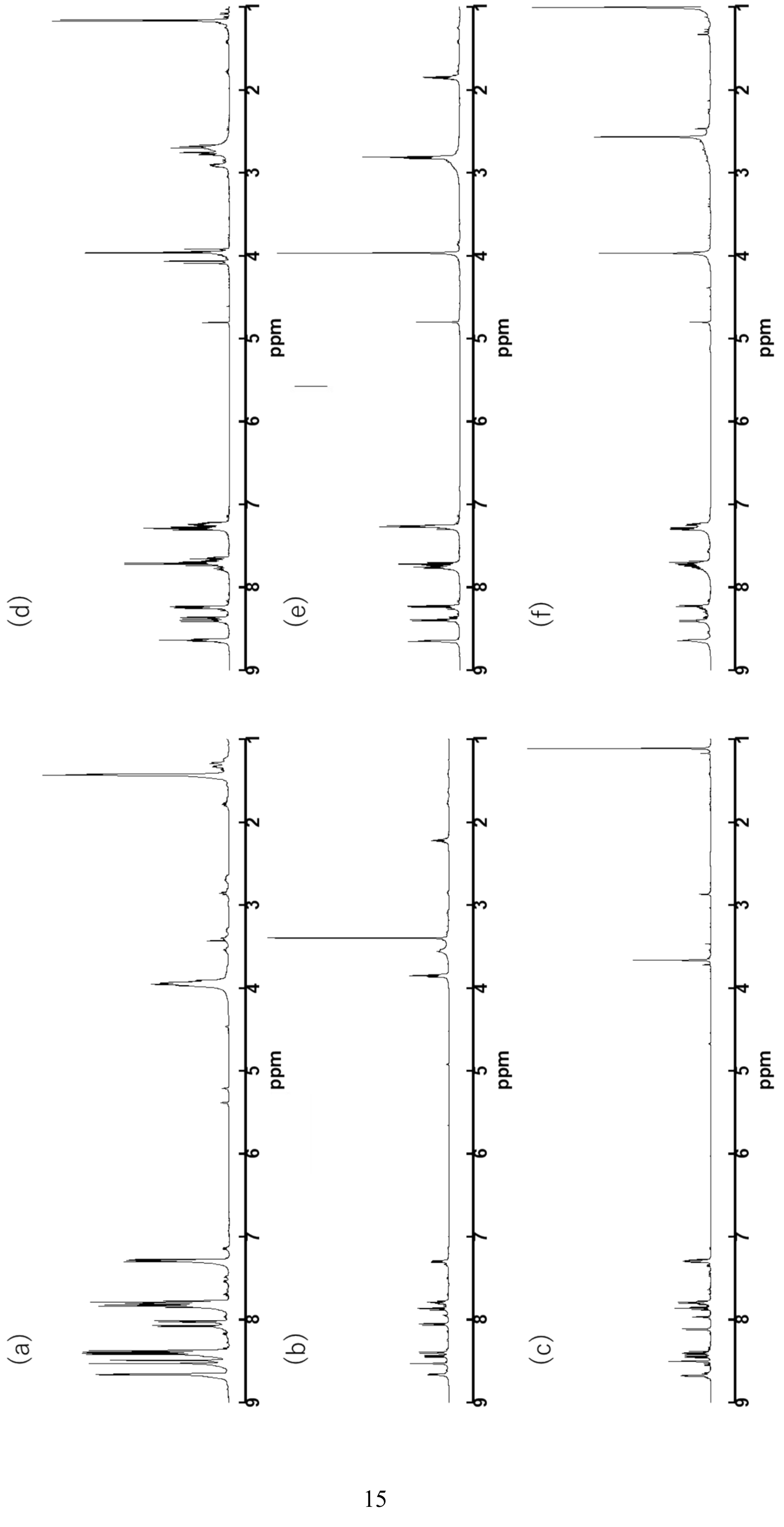

References

[1] M. Hasegawa, H. Ohtsu, D. Kodama, T. Kasai, S. Sakurai, A. Ishii and K. Suzuki, *New J. Chem*., 2014, 38, 1225. and CCDC 919427.

[2] R. Pavithran, N. S. S. Kumar, S. Biju, M. L. P. Reddy, S. Jr. Alves, R. O. Freire, *Inorg. Chem*., **2006**, *45*, 2184.

[3] C. Reichart (1988) "Solvents and Solvent Effects in Organic Chemistry, 2nd revised and enlarged edition", pp. 365–371. VCH, New York.

[4] W. T. Carnall, P. R. Fields and K. Rajnak, *J. Chem. Phys*., **1968**, *49*, 4450.

[5] G. H. Dieke and H. M. Crosswhite, *Appl. Optics*, **1963**, *2*, 675.